MANTECH Publications

Journal of Current Trends in Electrical Engineering

Volume 1, Issue 2, May-August, 2016

A Direct Torque Controlled Doubly-Fed Induction Motor with MPPT Enabled PV for Wide Constant Torque Region Operation

Sheenu V S[1], Jomole Joseph P[2]

PG Student (PCD) [1], Assistant Professor[2]

Department of EEE

Mar Baselios College of Engineering and Technology, Trivandrum

Corresponding Author: *vs21sheenu@gmail.com*

Abstract

A Direct Torque control algorithm which enables the Doubly Fed Induction Motor (DFIM) to operate in constant torque region is proposed here. This algorithm is employed for EV/HEV application. Inverters are supplied by a MPPT enabled PV and battery. Torque and air-gap flux of a DFIM can be controlled directly.

Keywords: *Doubly fed induction motor (DFIM), Electric vehicle/hybrid electric vehicle (EV/HEV), PV array (Photovoltaic Array)*

I. INTRODUCTION

Doubly- Fed Induction Machines are used as motor as well as generators. Wound-rotor induction machines with stator and rotor connected to separate ac sources having different frequencies are said to be doubly-fed machines. Doubly-Fed Induction Motor (DFIM) is mainly used for the application of electric propulsion systems because of its attractive features like ability to operate in the wide torque region. It can also be used to drive variable-speed pumps.

High speed operation of doubly-fed motor is comparatively different from that of singly-fed Induction Motors. For the purpose of comparison we assume that the base speed and torque production of DFIM are designed the same as those of Interior Permanent Magnets (IPM) and Induction Motors (IM).Moving to higher speeds

beyond the base speedω_b, the DFIM can maintain the same operational frequency for the first winding while increasing the operational frequency of the other for operating in super synchronous speed. The second winding frequency can increase until the induced voltage in the second winding reaching the maximum voltage at 2ω_b. This argument can also be applied to the speed range higher than 2ω_b where the flux weakening and constant power operation starts. In this way, the torque and constant power are all doubled.

It is worth pointing out that while doubling the torque-speed region, the current levels and, thus, copper losses of both windings are unchanged. Also true is that the stator core losses are not changed while the rotor core losses could be more than that of the IPM and IM but with a big benefit of doubling both the output speed and torque. It is reasonable to derive that a doubly-fed motor will have larger and balanced contour of high energy efficiency than that of both IPM and IM motors, especially at speeds higher than the base speed. A higher energy efficiency of doubly-fed motor in EV/HEV application directly contributes to a better fuel utilization and extended driving distance.

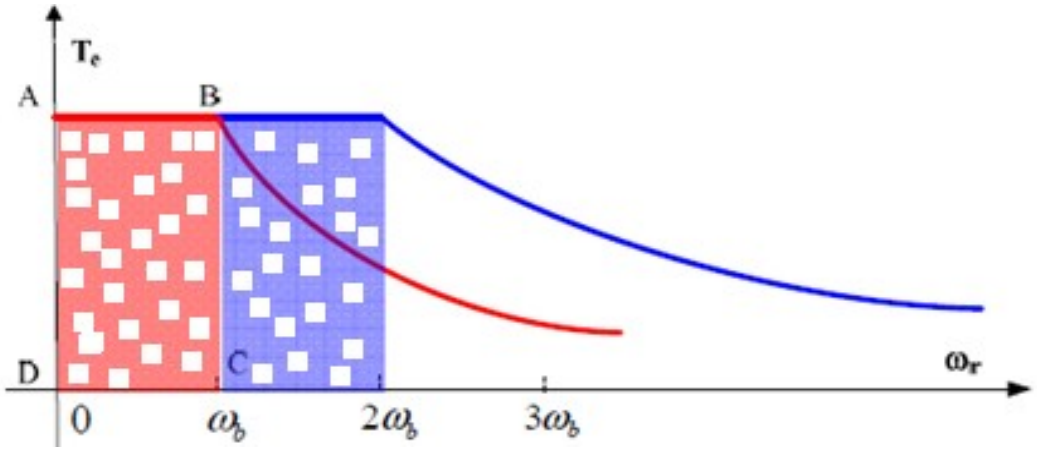

Fig.1.1 Comparison of torque-speed region of doubly fed motor to that of singly-fed motor.

II. DYNAMIC MODEL AND CONTROL STRATEGY FOR DFIM

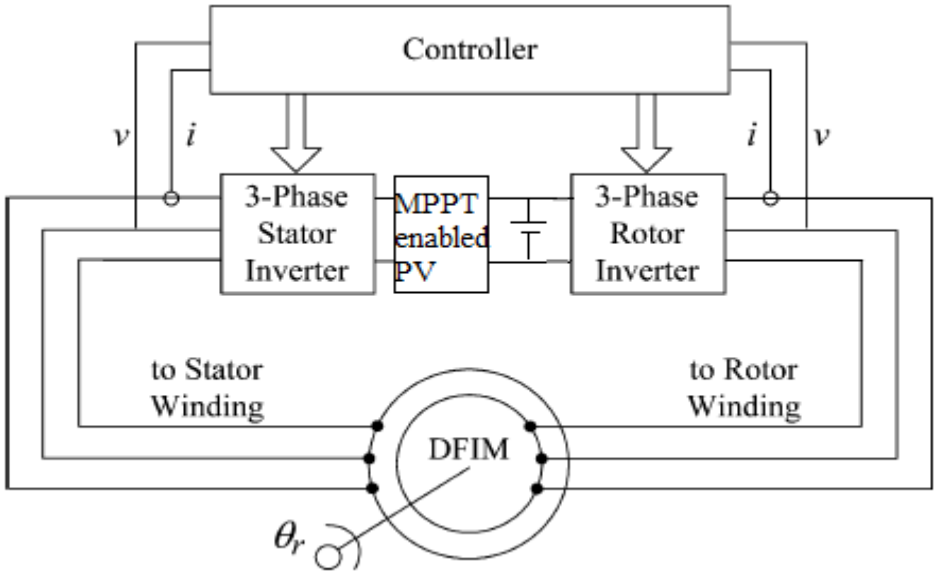

Fig.2.1 DFIM Drive system.

In the fig.2.1 shown above, there is a back-to-back converter is used for the doubly-fed motor to draw/send power from/to the battery pack. When compared with the power electronic circuits in singly-fed IM and IPM systems, the only difference is the system has two sets of three-phase inverter, one connected to stator side and other connected to rotor side. Because of the two inverters share the same battery pack with a common dc bus voltage, they can be operated separately. That means, both stator and rotor windings can be controlled independently. The power to the battery is supplied by a MPPT enabled photovoltaic array.

The modelling of PV is given in the next section.

The dynamic equations for the modelling of DFIM are given below.

$$V_{ds} = R_s i_{ds} + \frac{d\lambda_{ds}}{dt} - \omega_s \lambda_{qs} \qquad (2.1)$$

$$V_{qs} = R_s i_{qs} + \frac{d\lambda_{qs}}{dt} - \omega_s \lambda_{ds} \qquad (2.2)$$

$$\lambda_{ds} = L_s i_{ds} + L_m i_{dr} \quad (2.3)$$

$$\lambda_{qs} = L_s i_{qs} + L_m i_{qr} \quad (2.4)$$

$$V_{dr} = R_r i_{dr} + \frac{d\lambda_{dr}}{dt} - \omega_r \lambda_{qr} \quad (2.5)$$

$$V_{qr} = R_r i_{qr} + \frac{d\lambda_{qr}}{dt} + \omega_r \lambda_{dr} \quad (2.6)$$

$$\lambda_{dr} = L_r i_{dr} + L_m i_{ds} \quad (2.7)$$

$$\lambda_{qr} = L_r i_{qr} + L_m i_{qs} \quad (2.8)$$

$$T_e = 1.5p \frac{L_m}{L_s} \lambda_{qs} i_{dr} - \lambda_{ds} i_{qr} \quad (2.9)$$

$$\omega_{mr} = \frac{1}{p} \omega_{er} = \frac{1}{p} \omega_s + \omega_r \quad (2.10)$$

III. MODELLING OF PV CELL

A 250W PV module is modelled here. The equivalent circuit of a solar photovoltaic cell is shown in fig.3.1

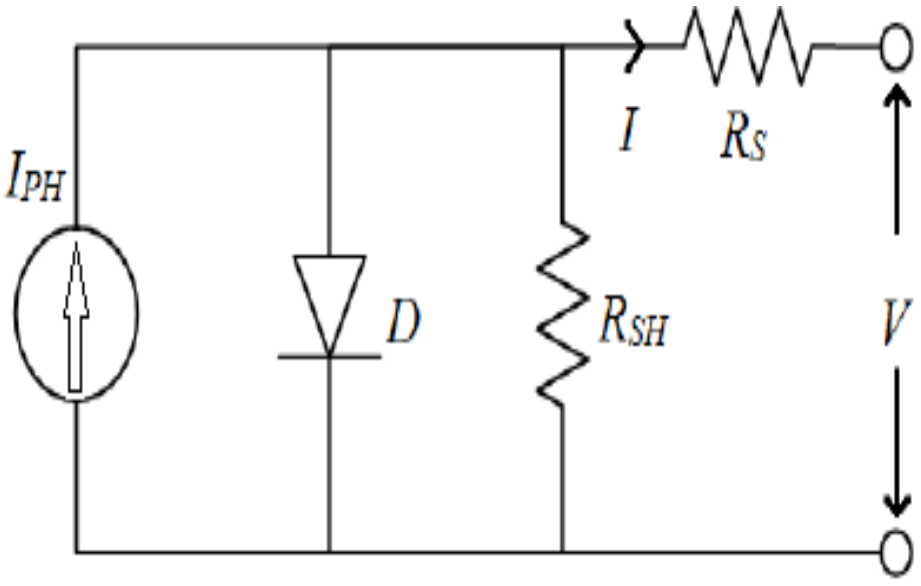

Fig.3.1 Equivalent circuit of a solar cell.

An equation of current to the load can be obtained from the equivalent circuit in Fig.3.1. The load current equation is given by

$$I = I_{PH} - I_S \exp\frac{q\ V + IR_s}{NKT} - 1 - \frac{V + IR_s}{R_{SH}} \quad (3.1)$$

In this equation, I is the load current,I_PHis the photocurrent, I_Sis the diode saturation current, q is the electron charge, V is the terminal voltage of the cell, N is the diode ideality factor, K is the Boltzmann constant, T is the cell temperature, R_sand 〖R〗_SHis the series and shunt resistance respectively. So, the behaviour of a solar photovoltaic (PV) cell is completely dependent on these parameters.

The above model of PV cell in Fig.3.1 includes two major subsystems that play a great effect on the behaviour of PV module. One of them calculates the photocurrent, I_PH. The photocurrent,I_PHdepends on the solar irradiance and cell temperature. The output of the PV module varies as a function of solar irradiance level which can be obtained from the following equation 3.2.

$$I_{PH} = I_{SC} + K_i\ T - T_{ref}\ \frac{B}{1000} \quad (3.2)$$

Here, $I_{SC}$is the short circuit current, K_i is the temperature coefficient of short circuit current, T is the cell T_{ref} is the reference temperature and B is the solar irradiation in m^2.

Generally the typical value of series resistance of the PV cell, $R_S$is very low. This model was developed to render the suitable model for any given PV cell so that it is possible to vary $R_S$and observe its effects on the behaviour of the PV module. This simulation was performed for three different values of R_S, respectively 1mΩ, 5mΩ and 10mΩ. The simulation was performed under the standard test condition (STC), where temperature, *T* was kept constant at °C (298K) and solar irradiation level, *B* was kept constant m^2.

In general, the value of the shunt resistance, R_{SH} of the PV cell should be large enough to achieve the maximum output from the PV module.

IV. IMPLEMENTATION OF THE PROPOSED ALGORITHM

In the constant torque region, our aim is to provide faster dynamic response and sufficient torque. To achieve this requirement the proposed algorithm keeps

the maximum allowable air-gap flux without core saturation.

In the constant power region, the aim is to control level of flux weakening. If it is not controlled, stability problems may occur. By controlling magnetizing current, the air-gap flux can be controlled directly. The air-gap flux weakening control of the DFIM is obtained by reducing magnetizing current. Reduction of magnetizing current can be achieved by controlling angle δ, where δ is the current phase shift angle. δ can be calculated by the following equation.

$$\delta = \cos^{-1}\left(\frac{i_m^2 - i_s^2 - i_r^{s'2}}{2 i_s i_r^{s'}}\right) \qquad (4.1)$$

V. OPERATION

The 3-phase stator currents of Doubly Fed Induction Motor are given to a Clark's transformation block. This block converts 3-phase currents to 2- phase α,β currents. 2-phase α,β currents are given to a Park's transformation block, which converts α,β currents to d,q currents. This d,q stator currents are then compared with the I_sd^* and I_sq^* components. The two current outputs from comparator are converted to corresponding voltage components by using a PI controller. This d,q voltages are given to an Inverse Park's Transformation block and get the corresponding 2-phase α,β voltages. These voltages are given to the SVPWM inverter in order to produce pulses. These pulses are again given to the DFIM for the closed loop operation.

The same operation explained above is takes place in the rotor side. ***See Table 1.***

VI. SIMULATION AND RESULTS

A. Simulation

Simulation diagram for DFIM with each inverter on stator and rotor side is shown in Fig.6.1.Inverter is supplied by a PV and battery.

Table 5.1 shows the rating and parameters of DFIM.

Parameter	Rated values
Power(kW)	30
Voltage(V)	415
Current(A)	100
Number of poles	4
Frequency(Hz)	50
Speed(rpm)	1500
Torque(Nm)	191
Nominal stator phase current	3.6A
Nominal rotor phase current	6.0A
Stator/rotor resistance	2.85/1.25Ω
Stator/rotor leakage inductance	22.4/12.8mH
Mutual inductance	164.6mH

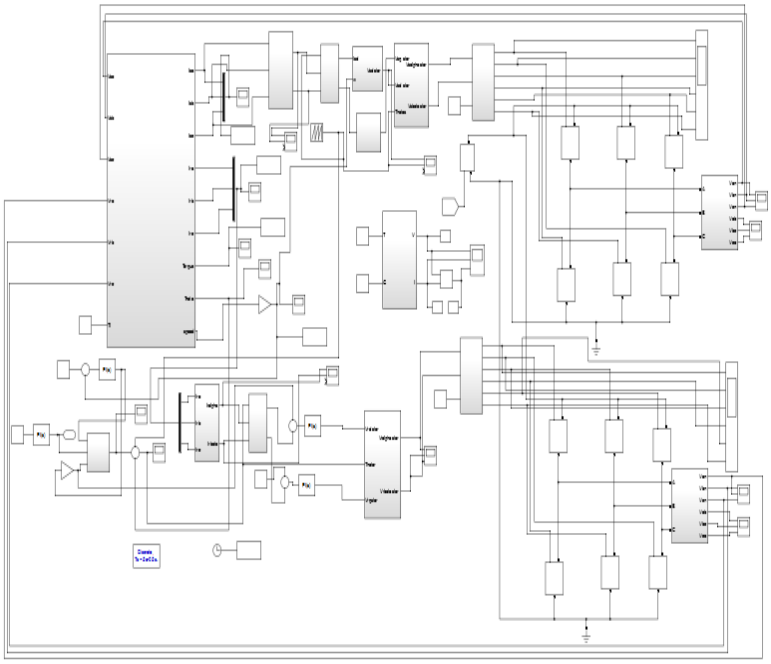

Fig.6.1 Simulation diagram.

B. Results

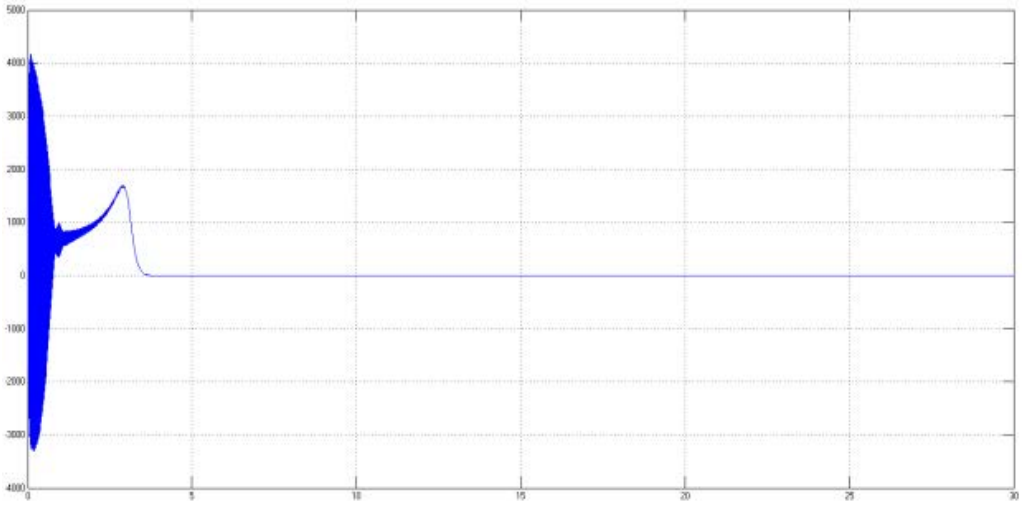

Fig.6.2 Torque characteristics of DFIM (X-axis: Time (s), Y-axis: Torque(Nm))

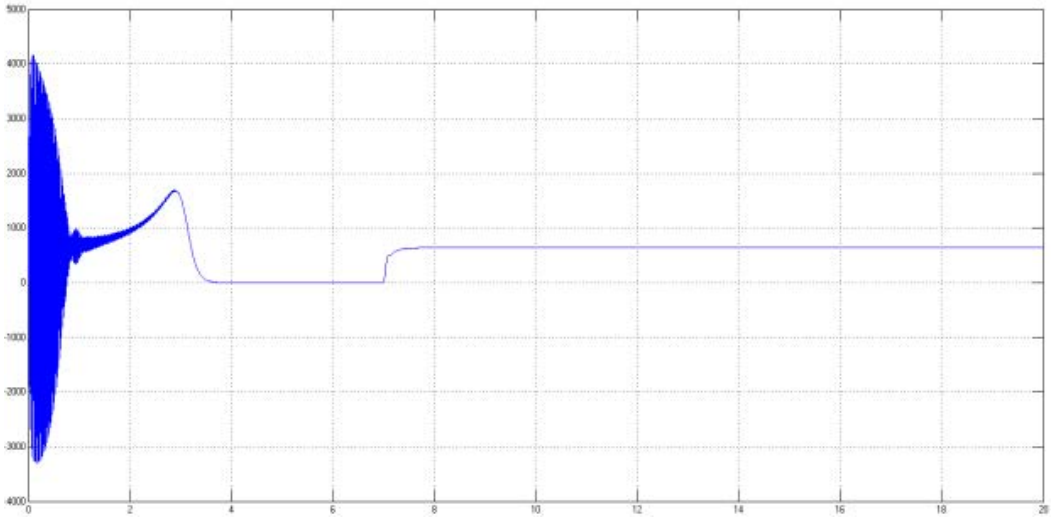

Fig.6.3 Torque vs Time when the load torque applied is 700Nm(X-axis:Time (s), Y-axis: Torque(Nm))

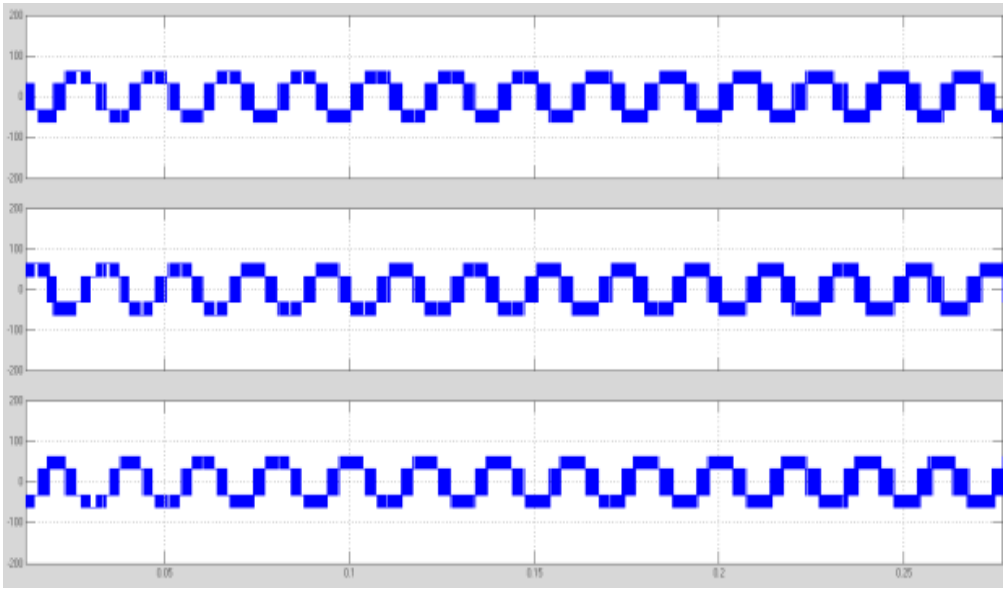

Fig.6.4 Phase voltage from the stator side Inverter (Y-axis: phase voltage (V), X-axis(Time(s))

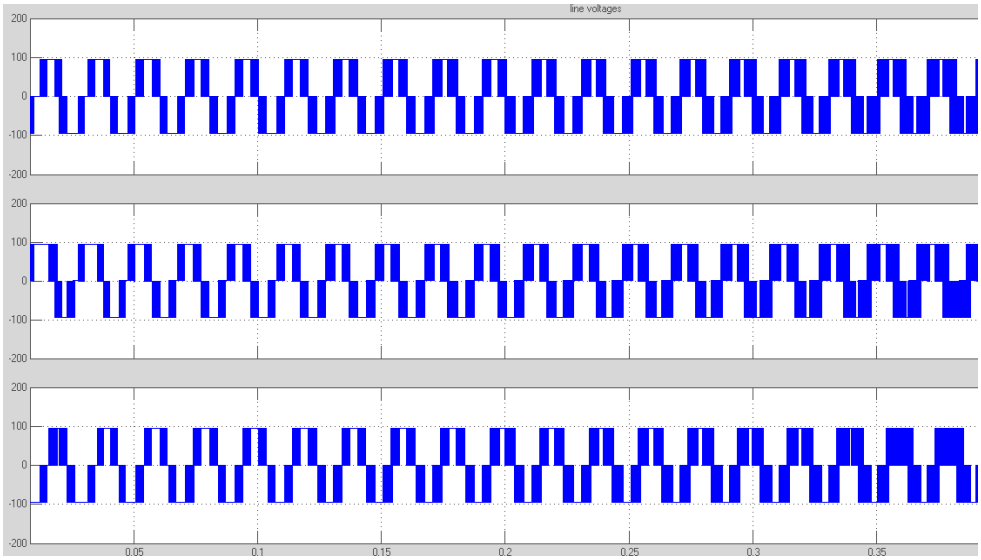

Fig.6.5 Line voltage from the stator side Inverter (X-axis:Time(s), Y-axis: Line voltage (V))

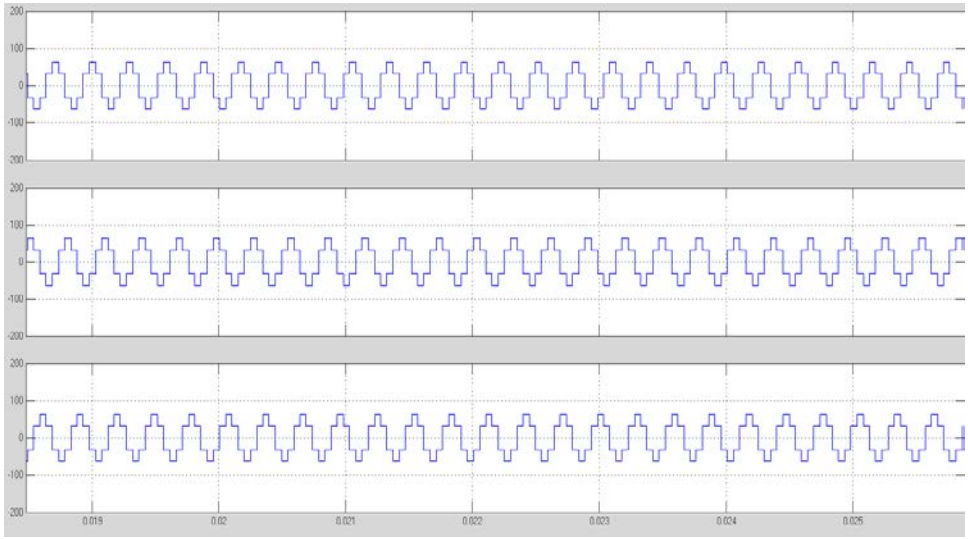

Fig.6.6 Phase Voltage from the rotor side inverter (X-axis:Time(s), Y-axis: phase voltage (V))

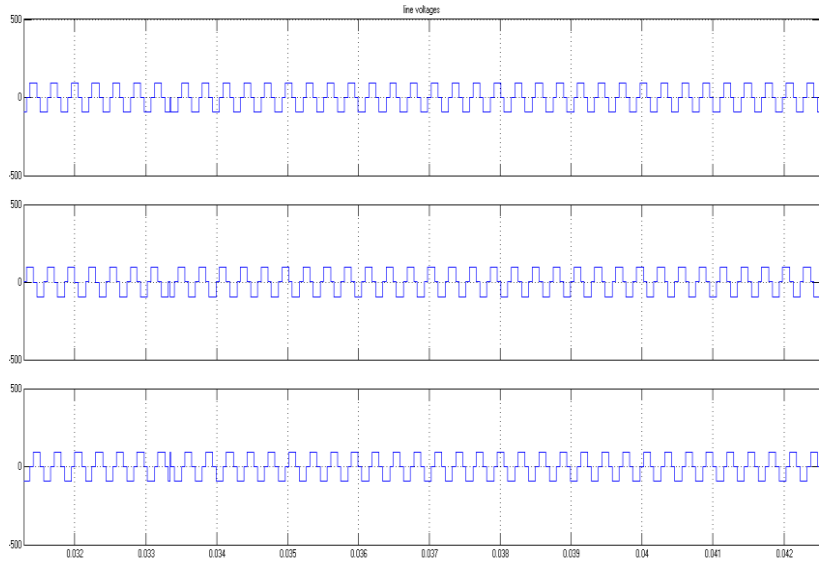

Fig.6.7 Line voltage from the rotor side inverter (X-axis: Time(s), Y-axis:Line voltage (V))

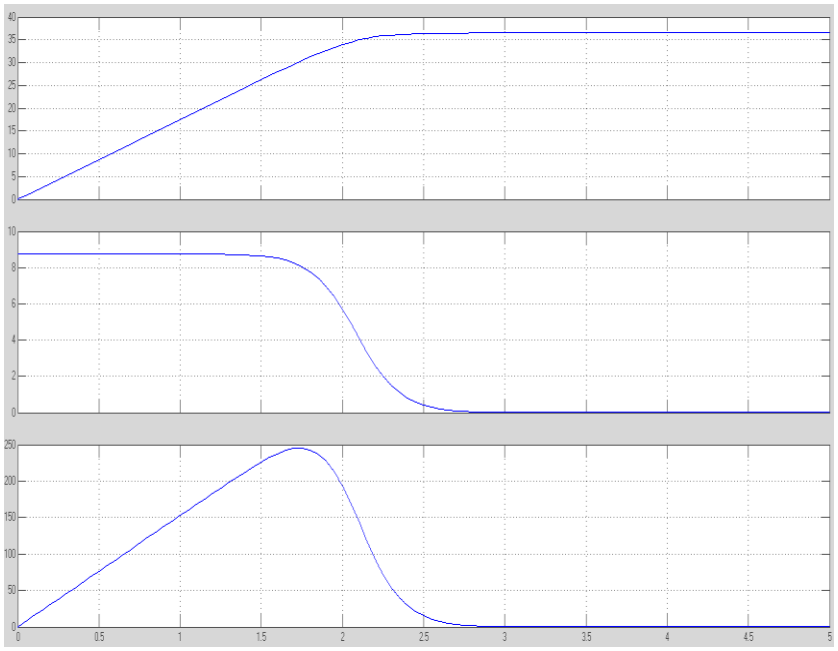

Fig.6.8 Output obtained from PV array (Y-axis: output voltage (V), output current (A), output power (W), X-axis: Time(s)).

CONCLUSION

This paper introduces a new control algorithm for the proper control of doubly fed induction motor for Electric Vehicle/Hybrid Electric Vehicle applications. There are some advantages for this algorithm.

1) Torque and air-gap flux of the DFIM can be controlled directly in both constant torque and constant power region. This is made possible by controlling two current vectors.

2) Efficiency of DFIM is controlled here.

3) When this algorithm is applied in a DFIM, the total system has less dependence on motor parameters than other type of control algorithms.

REFERENCES

1) Yu Liu, student member, IEEE ,and Longya Xu, fellow,IEEE, "The dual-current -loop controlled Doubly Fed Induction Motor for EV/HEV Applications" IEEE Transactions On Energy Conversion,Vol.28,no.4,pp.1045105 2,Dec2013.

2) G. Pellegrino, A. Vagati, B. Boazzo, and P. Guglielmi, "Comparison of induction and PM synchronous motor drives for EV application including design examples," IEEE Trans. Ind. Appl., vol. 48, no. 6, pp. 2322–2332, Nov./Dec. 2012.

3) M. Zeraoulia, M. E. H. Benbouzid, and D. Diallo, "Electric motor drive selection issues for HEV propulsion systems: A comparative study," IEEETrans. Veh. Technol., vol. 55, no. 6, pp. 1756–1764, Nov. 2006.

4) Y. Kawabata, E. Ejiogu, and T. Kawabata, "Vector-Controlled double inverter-fed wound-rotor induction motor suitable for high-power drives,"IEEE Trans. Ind. Appl., vol. 35, no. 5, pp. 1058–1066, Sep./Oct. 1999.

5) F. Bonnet, P. Vidal, and M. Pietrzak-David, "Dual direct torque control of doubly fed induction machine," IEEE Trans. Power Electron., vol. 54, no. 5, pp. 2482–2490, Oct. 2007.

6) L. Xu and Y. Liu, "Comparison study of singly-fed electric machine with doubly-fed machine for EV/HEV applications," in Proc. IEEE Int. Conf.Elect. Mach. Syst., 2011, pp. 1–5.

7) Leon.M.Tolbert, "Simulink Implementation Of Induction Machine Model –A Modular Approach" Dept.of Electrical Engineering, University Of Tennesse. pp.728-734.